Journal of Controlled Release 319 (2020) 222–233

Contents lists available at ScienceDirect

Journal of Controlled Release

journal homepage: www.elsevier.com/locate/jconrel

Indium-111 labelling of liposomal HEGF for radionuclide delivery via ultrasound-induced cavitation

Joshua Owen[a,*], Eloise Thomas[b], Jyothi Menon[b,c], Michael Gray[a], Irini Skaripa-Koukelli[b], Martin R. Gill[b], Sheena Wallington[b], Rebecca L. Miller[d], Katherine A. Vallis[b,1], Robert Carlisle[a,1]

[a] Department of Engineering Science, Institute of Biomedical Engineering, University of Oxford, Old Road Campus Research Building, Oxford OX3 7DQ, UK
[b] CRUK/MRC Oxford Institute for Radiation Oncology, Department of Oncology, University of Oxford, Old Road Campus, Oxford OX3 7DQ, UK
[c] College of Pharmacy, The University of Rhode Island, Kingston, RI 02881, USA
[d] Department of Cellular and Molecular Medicine, University of Copenhagen, Blegdamsvej 3B, 2200 Copenhagen N, Denmark

ARTICLE INFO

Keywords:
Ultrasound
Nanoparticles
Radiotherapy
Radiopharmaceuticals
Liposomes
Enhanced delivery
Cavitation

ABSTRACT

The purpose of this exploratory study was to investigate the combination of a radiopharmaceutical, nanoparticles and ultrasound (US) enhanced delivery to develop a clinically viable therapeutic strategy for tumours overexpressing the epidermal growth factor receptor (EGFR). Molecularly targeted radionuclides have great potential for cancer therapy but are sometimes associated with insufficient delivery resulting in sub-cytotoxic amounts of radioactivity being delivered to the tumour. Liposome formulations are currently used in the clinic to reduce the side effects and improve the pharmacokinetic profile of chemotherapeutic drugs. However, in contrast to non-radioactive agents, loading and release of radiotherapeutics from liposomes can be challenging in the clinical setting. US-activated cavitation agents such as microbubbles (MBs) have been used to release therapeutics from liposomes to enhance the distribution/delivery in a target area. In an effort to harness the benefits of these techniques, the development of a liposome loaded radiopharmaceutical construct for enhanced delivery via acoustic cavitation was studied. The liposomal formulation was loaded with peptide, human epidermal growth factor (HEGF), coupled to a chelator for subsequent radiolabelling with ^{111}Indium ([^{111}In]In^{3+}), in a manner designed to be compatible with preparation in a radiopharmacy. Liposomes were efficiently radiolabelled (57%) within 1 h, with release of ~12% of the radiopeptide following a 20 s exposure to US-mediated cavitation *in vitro*. In clonogenic studies this level of release resulted in cytotoxicity specifically in cells overexpressing the epidermal growth factor receptor (EGFR), with over 99% reduction in colony survival compared to controls. The formulation extended the circulation time and changed the biodistribution compared to the non-liposomal radiopeptide *in vivo,* although interestingly the biodistribution did not resemble that of liposome constructs currently used in the clinic. Cavitation of MBs co-injected with liposomes into tumours expressing high levels of EGFR resulted in a 2-fold enhancement in tumour uptake within 20 min. However, owing to the poor vascularisation of the tumour model used the same level of uptake was achieved without US after 24 h. By combining acoustic-cavitation-sensitive liposomes with radiopharmaceuticals this research represents a new concept in achieving targeted delivery of radiopharmaceuticals.

1. Introduction

Targeted radionuclide therapy (TRT) combines the specificity of tumour seeking carriers with the toxicity of radioisotopes [1]. There are several examples of this approach in clinical use such as ^{177}Lutetium-Dotatate for neuroendocrine tumours [2], and ^{177}Lutetium-prostate-specific membrane antigen (PSMA inhibitor) for metastatic castration-resistant prostate cancer [3]. However, both these strategies rely on ^{177}Lutetium which emits high energy electrons (beta-particles) with a track length in the centimeter range which can lead to off target effects [4]. One promising strategy for TRT is the use of radionuclides that decay through electron capture and the release of short track-length (< 30 μm), moderately high linear energy transfer (LET) electrons that cause very localised damage and few unwanted off-target effects [4]. To cause cancer cell death these radionuclides must enter the nucleus in sufficient quantity to give rise to irreparable DNA damage. The

* Corresponding author.
E-mail address: owenjw@cc.nih.gov (J. Owen).
[1] Both authors contributed equally.

https://doi.org/10.1016/j.jconrel.2019.12.045
Received 11 July 2019; Received in revised form 24 December 2019; Accepted 27 December 2019
Available online 28 December 2019
0168-3659/

conjugation of such radionuclides to carriers with cell-penetrating and/or nuclear localizing sequences offers a route to enhanced selectivity [4,5]. A previously tested example of this strategy is the use of [^{111}In]In^{3+}, which decays through electron capture, tagged to the HEGF peptide ([^{111}In]In-HEGF) which binds to the EGFR that is overexpressed by a range of solid cancers. Crucially, following binding of HEGF, the EGFR translocates to the nucleus, delivering [^{111}In]In^{3+} to the site where its decay can impact cell survival most effectively [6]. However, a notable limitation of this approach is that the small size of peptide-based radiopharmaceuticals renders them susceptible to rapid renal clearance giving rise to unfavourable circulation kinetics [7]. This can often result in insufficient accumulation of radionuclides within tumours [8]. Also in the case of small peptides reabsorption and retention in the proximal tubules after glomerular filtration can cause a high radiation dose in the kidneys therefore lowering the administered dose for small peptide radiopharmaceuticals is desirable [9]. Molecularly targeted agents such as peptides are also limited by low payloads and insufficient delivery of radioactivity to the tumour [10] as well as causing side effects such as flushing, chills, nausea, and vomiting [11]. EGFR is apparent in some of the most frequent cancers but the benefits of small agents for anti EGFR therapy plus cytotoxic agents have yet to appear [12].

Nanoparticles can be designed for drug delivery and may be fabricated from natural or synthetic compounds [7]. Nanoparticle delivery systems have been shown to reduce the cytotoxicity of low molecular weight chemotherapeutics and provide greater anticancer efficacy [13]. This means dosing need not be limited by the risk of severe adverse effects in non-target tissue [14]. Liposomes are a class of nanoparticle which are particularly suited to cancer therapy as they are easy to produce and can encapsulate a large payload of active therapeutics within the aqueous core of their spherical lipid bilayer. Furthermore, it is possible to surface modify liposomes with polyethylene glycol (PEG) [15] to provide protection from reticuloendothelial system (RES) mediated clearance. Drug encapsulating liposomal formulations can therefore dramatically extend the blood circulation time compared to free drug. In turn, this may allow passive accumulation and retention in tumours through the enhanced permeability and retention (EPR) effect [16], and although the true extent of the EPR effect is contentious [17] there is pre-clinical and clinical data in support of the improved efficacy it provides. Specifically, Doxil®, which was the first liposome formulation to be approved for clinical use [18,19] demonstrates a clearance rate in humans of approximately 0.1 L/h, compared to 45 L/h for unencapsulated doxorubicin [18,20]. Liposomes can be produced by a variety of techniques [21,22]. Although liposomal formulations are currently available in the clinic for delivery of chemotherapeutics [18], they have not been used clinically for the delivery of radioisotopes.

The application of liposomes to the delivery of radioisotopes therefore appears ripe for exploitation, although, there are key factors limiting the success of such a strategy. Firstly, the timescale of the conventional process of liposome formulation, loading and purification is not always compatible with the timescale and working practice required when using radioisotopes clinically. Most research has focused on decorating the surface of nanoparticles with radiopharmaceuticals [23,24]. Although, methods to load radioactive compounds and radiopharmaceuticals into liposomes have also been developed previously, these techniques have substantial limitations that must be overcome before achieving clinical translation [23,25–29]. For example, freeze thaw was used to load ^{99m}Technetium-ceftizoxime into liposomes. However, the half-life of technetium is 6 h and freeze thaw cycles typically take multiple hours and require techniques and equipment which are not always readily available in a hospital environment [30]. Pre-loading of liposomes with a radioisotope at a manufacturing site would create transport and storage times that would compromise the amount of radioactivity available by the time of use. Methods of encapsulating radioisotopes in a more clinically viable fashion have been developed via loading of ^{64}Copper, ^{52}Manganese and [^{111}In]In^{3+} into liposomes [31–33]. Furthermore, most research reported to date, has sought to encapsulate the radioisotope without providing mechanisms for cancer cell targeting, release from the liposome or for trafficking of the radionuclide to the nucleus once release from the liposome has occurred [34]. Therefore, these constructs become entirely dependent on the EPR effect for tumour selectivity, with no means of either releasing the payload from the liposome or ensuring penetration from the perivascular regions into and throughout the tumour mass.

To address the above challenges, we describe a long-term-storage compatible 'platform' liposome loaded with DTPA-HEGF which can be easily post-loaded with [^{111}In]In^{3+} just prior to clinical administration. Furthermore, by ensuring the liposome formulation is responsive to US-mediated cavitation events, it is possible to achieve temporal and spatial control of radiopharmaceutical cargo release [14]. Indeed, ultrasound, a longitudinal pressure wave of frequency > 20 kHz, can be efficiently delivered through the body and localised to millimetre scale tissue domains when using low MHz frequencies, exposing them to alternating compression and rarefaction cycles of microsecond duration. These waves can create cavitation events, i.e. the expansion and collapse of a gas bubble from pre-formed cavitation nuclei such as a shelled microbubble, which can be co-delivered with the therapeutic into the blood stream [35]. The mechanical action of such cavitation events can increase the permeability of cell membranes, and/or selectively disrupt the membranes of liposomes [14,36,37]. Hence, whilst in conventional drug delivery systems the drug is limited to the perivascular region and transport is controlled by diffusion [36], US-mediated-cavitation used in combination with cavitation responsive carriers can provide a powerful and safe mechanism to overcome tumour delivery barriers by providing site-specific triggered drug release and enhanced delivery.

In this study, the aim was to determine if a cavitation sensitive liposome loaded with a radiopeptide has clinical potential. We have developed a clinically relevant method of afterloading [^{111}In]$InCl_3$ into cavitation sensitive liposomes for radiolabelling of encapsulated DTPA-HEGF, a tumour-targeting peptide, for enhanced delivery/triggered release as represented in Fig. 1. The methods used at each stage are based on existing techniques, for ease of translation: [^{111}In]In^{3+} labelled HEGF ([^{111}In]In-HEGF) has been tested in humans [11], the liposome formulation is based on those used clinically, and MBs are also currently used in the clinics, although only as US contrast agents to date.

2. Materials and methods

2.1.1. Preparation of HEGF

The conjugation of HEGF (Life Sciences, Thermo Scientific, Loughborough, UK) with diethylenetriaminepentaacetic dianhydride 98% (DTPA) (Sigma Aldrich, Gillingham, UK) was carried out as previously described [38]. Briefly, HEGF (1 mg) was dissolved in sodium bicarbonate (pH 8.3) (400 μL), DTPA (5 × molar excess) was added in DMSO (dimethyl sulfoxide) (30 μL) and incubated for 45 min at room temperature (RT). This solution was then eluted through a Sephadex G25 (Sigma Aldrich, Gillingham, UK) column and the amount of protein recovered in each aliquot (100 μL) was analysed using a Nanodrop spectrophotometer (Thermo Scientific, Wilmington, DE). HEGF was centrifuged (12,300 ×*g*) in a molecular weight cut off (3 kDa) ultrafiltration tube (Amicon®, Sigma Aldrich, Gillingham, UK) three times in 0.1 M citrate buffer (pH 5.0). This was then stored at 4 °C for later encapsulation in liposomes.

2.1.2. Synthesis of liposomes

All lipids were purchased from Avanti Polar Lipids, Alabaster, Alabama, USA. For the liposome formulation, 1,2-dipalmitoyl-sn-

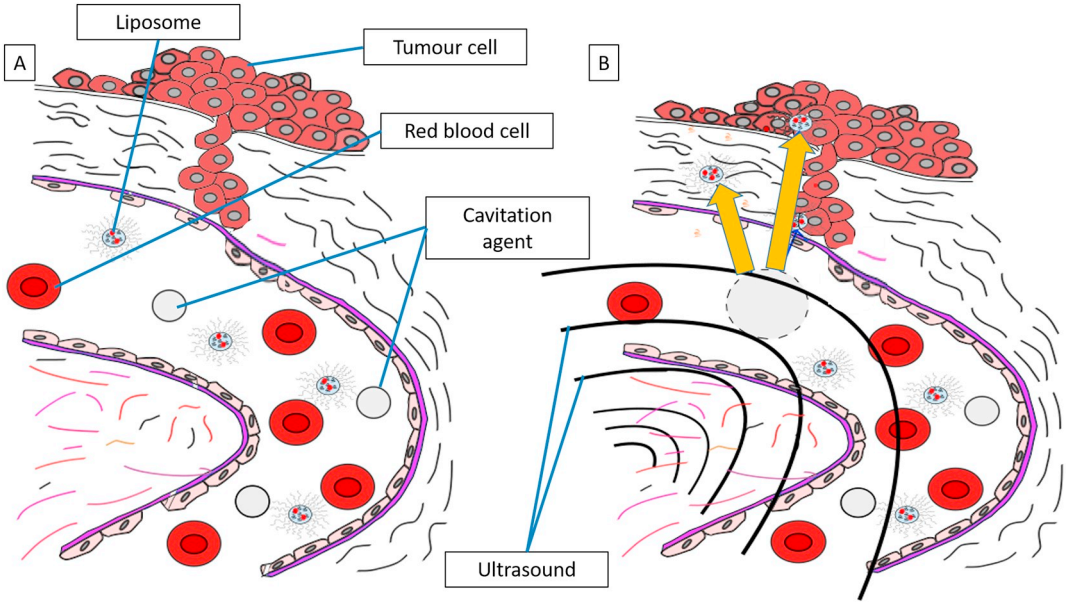

Fig. 1. A) *in vivo* schematic of tumour cells adjacent to a blood vessel with cavitation agents and [^{111}In]In-HEGF loaded liposomes and B) application of US induced cavitation to drive liposomes into tumour tissue and to release [^{111}In]In-HEGF to interact with EGFR. Objects shown in the diagram are not drawn to scale, liposomes are 175 nm whereas MBs are 2–8 μm.

glycero-3-phosphocholine (DPPC), 1-tetradecanoyl-2-octadecanoyl-sn-glycero-3-phosphocholine (MSPC), 1,2-distearoyl-sn-glycero-3-phosphoethanolamine-N-[methoxy(polyethylene glycol)-2000] DSPE-PEG(2000) at a molar ratio of (85:5:10) was used resulting in approximately 40 mg of lipid. The chloroform was removed under high vacuum for 3 h, using a vacuum pump (Edwards RV12, Edwards, West Sussex, UK) attached to a schlenk line (Glass Solutions, Watford, UK) via a cold trap (Glass Solutions, Watford, UK) immersed in liquid nitrogen, to leave a lipid film. Cyclohexane (2 mL) (Sigma Aldrich, Gillingham, UK) was added to the lipid film followed by vortexing, heating (50 °C) for 1 min, immersion in liquid nitrogen for 2 min and freeze drying over 2 days (− 50 °C and 100 mTorr) (Virtis Lyostar Advantage Plus EL-85) to produce a lipid powder unattached to the glass. HEGF (see above) (0.5 mg) was reconstituted in citrate buffer (pH 5.0) (200 μL) at a concentration of 10 mg/mL and this was added to the lipid powder. The lipid, HEGF solution was pipetted up and down using a 100 μL pipette to break up and disperse the lipids into vesicles. Citrate buffer (0.1 M, 100 μL) was added and the mixture was extruded 11 times through a 100 nm polycarbonate membrane (Avanti Polar Lipids, Colorado, USA) at 37 °C using a teflon mini-extruder (Avanti Polar Lipids, Colorado, USA) with 2 syringes (1 mL). The extruded liposomes were then centrifuged at 12,300 ×*g* for 15 min in phosphate buffered saline (PBS) (1 × concentration, pH 7.1) in a centrifuge tube (Amicon®, Sigma Aldrich, Gillingham, UK) with a molecular weight cut-off of 30 kDa for a minimum of three cycles to remove any excess non-encapsulated HEGF. Loading efficiency was assessed via High Performance Liquid Chromatography (HPLC) after SE centrifugation and ultracentrifugation (70,000 ×*g*, 30 min) to ensure removal of excess HEGF for accurate analysis of liposome loading [39]. Liposomes were then stored at 4–8 °C for later loading with [^{111}In]$InCl_3$. The liposome size was measured via dynamic light scattering (DLS) (Zetasizer Nano ZS, Malvern Instruments, Worcestershire, UK). Empty Liposomes underwent the same process but without addition of HEGF.

2.1.3. ^{111}In-labelling of HEGF loaded liposomes

HEGF-Lip in PBS (pH 7.5) were incubated with [^{111}In]$InCl_3$ (15 MBq) for 1 h at 38 °C, following which the [^{111}In]In-HEGF-Lip were separated from free [^{111}In]In^{3+} by two repeats of size exclusion centrifugation (MW cut off 30 kDa, 12,300 ×*g* for 20 min) (SE centrifugation). A CRC®-25R dose calibrator (Capintec, Inc., Florham Park, NJ) was used to measure the amount of radioactivity present in the filtrates and the collected liposomes. From mixing the HEGF liposome with [^{111}In]$InCl_3$ to obtaining the purified radiolabelled formulation took 2 h.

2.1.4. Characterisation of radiolabelled liposomes

To determine ^{111}In-labelling efficiency three samples were compared: 1) Empty Liposomes containing no HEGF, 2) non-purified liposomes: i.e. HEGF encapsulated within liposomes and HEGF in the solution outside the liposomes and 3) purified liposomes which had HEGF encapsulated within liposomes only. These three samples were loaded with [^{111}In]$InCl_3$ and cleaned twice using SE Centrifugation (MW cut off 30 kDa, 12,300 ×*g* for 20 min). The amount of associated radioactivity in the filtrates and liposome solutions was then compared using the CRC®-25R dose calibrator.

The radiochemical yield was determined by silica gel instant thin-layer chromatography (SG-ITLC) in 0.1 M sodium citrate buffer (pH 5.2). Radioactivity measurements of the silica strips were obtained using radio-TLC scanner (Eckert & Ziegler Radiopharma, Inc., Hopkinton, MA, USA).

2.1.5. Transmission electron microscopy

Liposome morphology was observed by placing an aliquot of the liposome solution (10 μL) on a 200-mesh Formvar-coated copper grid (Agar Scientific, Stansted, Essex), allowing it to air-dry and then negatively staining the sample with 2% *w/v* uranyl acetate and allowing further air drying. A transmission electron microscope (Tecnai T12, FEI, Hillsboro, OR) was used for image acquisition.

2.1.6. Dynamic light scattering (DLS)

The hydrodynamic diameter of liposomes was measured using DLS (ZetaSizer Nano, Malvern Instruments Ltd., Malvern, Worcestershire, UK). Liposome samples (10 μL) were added to 990 μL of PBS and each sample measured three times.

2.1.7. Reverse phase chromatography of liposome extracted HEGF

To determine the uptake of HEGF into liposomes, HEGF standard samples (1 μg, 10 μg and 40 μg) and HEGF-containing liposomes

(HEGF-lip) were separated using a C18 reverse phase (Supelco) column on a Shimadzu SPD 10A HPLC system (Shimadzu). All samples were suspended in 7% triton X-100 (Sigma Aldrich, Gillingham, UK) and incubated for 20 min, before buffer A (water with 0.1% formic acid) was added to give a final volume of 700 μL. Samples were centrifuged at 12,300 ×*g* for 20 min, the supernatant was then loaded onto a C18 column in buffer A and eluted from the column using eluent B (80% acetonitrile with 0.1% formic acid) on a gradient of 0–50% B in A over 20 min. DTPA-HEGF was monitored at an absorbance of 214 nm. Loading efficiency was determined using the following equation:

$$Loading\ Efficiency\ (\%) = \left(\frac{HEGF\ in\ Liposome\ (\mu g)}{HEGF\ stock\ (\mu g)}\right) \times 100 \quad (1)$$

2.1.8. Clonogenic assays

In vitro experiments were conducted on EGFR-high MDA-MB-468 (1.3×10^6 EGFR/cell) and EGFR-low MCF7 (1×10^4 EGFR/cell) cells cultured in Dulbecco's Modified Eagle's Medium (DMEM) supplemented with 10% fetal bovine serum (FBS) and 1% penicillin-streptomycin-glutamine (PSG). Cells were seeded in 35 mm, high μ-Dishes with a glass bottom (ibidi GmbH, Am Klopferspitz, Planegg/Martinsried) at a concentration of 2.5×10^5 cells/well in 2 mL of supplemented DMEM. These cells were left overnight to attach. The μ-Dishes were examined via light-field microscopy to determine cell attachment, the media was removed, 8 mL of supplemented DMEM was added and cells were exposed to combinations of [^{111}In]In-HEGF loaded liposomes ([^{111}In]In-HEGF-Lip) (1 MBq) and SonoVue™ MBs (200 μL) (sulphur hexafluoride microbubbles: Bracco Diagnostics Inc., Milan, Italy) (SV) to give a final microbubble concentration of 3.75×10^6 bubbles/mL, prior to US exposure as outlined in Table 1 below. A test group exposed to US in the absence of a MB agent (i.e. no cavitation) and the presence of [^{111}In]In-HEGF-Lip was not included here because previous studies with US alone with this formulation had shown it to provide no release unless cavitation was instigated [14]. See Supplementary Figs. 1 and 2 and Supplementary Information (*ultrasound system characterisation*) for US details and characterisation. Cells were incubated for 24 h in the same medium, washed twice with PBS, detached with Trypsin-EDTA (0.05%), phenol red (1 mL) (Thermo Scientific, Loughborough, UK) and seeded in a 6-well plate at multiple seeding densities (500, 1000 and 2000 cells/ well). After 14 days, colonies were fixed and stained using 1% methylene blue mixture in methanol. Colonies were counted using a GelCount automated colony counter (Oxford Optronix, Oxford, UK).

2.1.9. Liposomal release in response to ultrasound

Liposomes were exposed to US as described in the Supplementary Information. [^{111}In]In-HEGF-Lip (5 MBq) were added to sealed plates with SV (1 mL) and exposed to US or a sham exposure at the same conditions as the clonogenic assays. After 2 h, 1 mL of the sample was removed and centrifuged in a molecular weight cut off (30 kDa) SE centrifuge tube (12,300 ×*g*, 20 min) and the total percentage of radioactivity in the filtrate was measured via a CRC®-25R dose calibrator (Capintec, Inc., Florham Park, NJ). The quantity of radioactivity that passed through the filters owing to liposome destruction in the SE centrifugation process was also measured and subtracted from the results.

Table 1
Samples used in clonogenic assays.

Sample name	Cavitation agent	Ultrasound	Liposomes containing [^{111}In]In-HEGF
Untreated			
US only		X	
MBs only	X		
MBs + US	X	X	
MBs + ([^{111}In]In-HEGF-Lip)	X		X
MBs + ([^{111}In]In-HEGF-Lip) + US	X	X	X

2.1.10. Cellular internalisation of radioactivity

MDA-MB-468 or MCF7 cells were prepared in Ibidi dishes in a similar manner to the clonogenic assays. Cells were exposed to [^{111}In]In-HEGF-Lip alone (1 MBq), SV alone (200 μL) or [^{111}In]In-HEGF-Lip (1 MBq) and SV (200 μL) with US. After 2 h the cells were washed and trypsinised and the amount of radioactivity measured using a gamma counter (HIDEX, Lemminkäisenkatu 62 FIN-20520 Turku, Finland). To consider cell concentration the protein content of the cells was then measured using the Bincinchoninic acid assay as per manufacturer's instructions (Pierce™ BCA Protein Assay Kit, Thermo Fisher Scientific, MA, USA).

2.1.11. Ethical statement

All procedures were conducted in accordance with the Animals Scientific Procedures Act of 1986 (UK) (Project License Numbers 30/3115 and P13B66CD9 issued by the Home Office). The protocols were approved by the Committee on the Ethics of Animal Experiments of the University of Oxford. All imaging was performed under 2–4% isoflurane anaesthesia delivered in oxygen enhanced room air (4% for induction of anaesthesia, ~2% for anaesthesia maintenance). Throughout imaging experiments, mice were maintained at 35–37 °C, respiration rate was monitored and all efforts were made to minimize suffering. Mice were housed (5 to 6 animals per cage) in individual ventilated polycarbonate solid-bottomed cages. Airflow within the cages was on a positive pressure and was controlled electronically by an IVC air handling system (Techniplast UK). A 12 h dark and light cycle was implemented with the ambient air temperature set at 21 °C ± 2 with 55% ± 10 humidity. All animals were provided with certified rodent diet, filtered water *ad libitum*, autoclaved bedding, nesting material and cage enrichment.

2.1.12. Animal preparation

Two mouse strains were used to complete the *in vivo* experiments. Athymic nude (NU(NCr)-Foxn1nu), and Severe Combined Immunodeficiency Disease (SCID) (CB17/Icr-Prkdc < scid > / IcrIcoCrl). Athymic nude and SCID mice were selected for their immunodeficient status and ability to support growth of human tumour cells. All mice were adult females, gender was selected based on the use of a breast cancer model. Mice entered study at approximately 40 days old. The mean start weight of athymic nude mice and SCID mice was 25 g and 16 g respectively. SCID mice were used for blood lifetime studies owing to their genetic similarity to athymic nudes and smaller size for use in the required SPECT imaging cradle.

All cancer cells were implanted subcutaneously into the right flank of the mice. MDA-MB-468 were injected at ~5 million cells/site with 50% matrigel (Thermo Scientific, Loughborough, UK) in serum free DMEM. MCF7 cells were not used *in vivo* due to animal welfare considerations owing to their requirement for estrogen supplementation. Where an indwelling cannula was used to administer contrast agents and treatments, a catheter (PE10, 0.28/0.64 mm internal/external diameter; Linton Instrumentation) was inserted into the lateral tail vein. Omniscan (gadodiamide, 0.5 M, 30 μL; GE Healthcare) was used as the contrast agent for Dynamic Contrast Enhanced Magnetic Resonance Imaging (DCE-MRI), and SonoVue™ (8 μL) was used for contrast imaging. All injections were performed manually except for injection of contrast agent for DCE-MRI where a syringe pump was used.

2.1.13. In vivo biodistribution

Athymic nude mice (6 weeks old) were anaesthetised (4% Isoflurane in air induction followed by 2% for maintenance). Animals were entered into a study when xenograft volume reached 70–100 mm^3. Mice (4 per group) received either [^{111}In]In-HEGF-Lip (6 MBq) or [^{111}In]In-HEGF (6 MBq) via intravenous (i.v.) injection into the lateral tail vein.

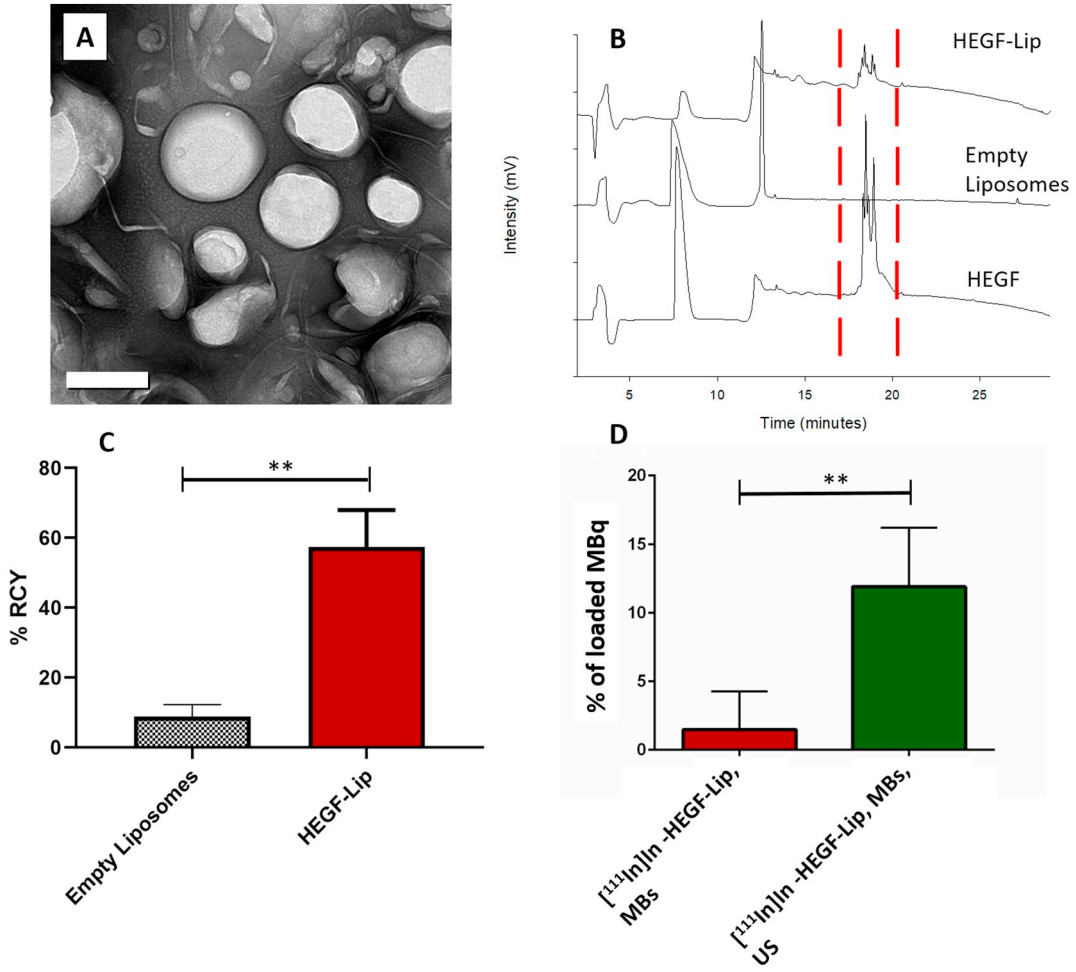

Fig. 2. Characterisation of liposomes. A) Transmission electron microscopy confirming the size and showing the morphology of the HEGF-Lip (scale bar = 100 μm). B) High Performance Liquid Chromotography analysis of HEGF, Empty Liposomes and HEGF-Lip cleaned by ultracentrifugation. C) ^{111}In-labelling efficiency of empty liposomes compared to liposomes containing HEGF, after addition of [^{111}In]$InCl_3$ (11 MBq) and 2 cycles of ultrafiltration ($n = 3$). D) Analysis of ^{111} In-HEGF release from [^{111}In]In-HEGF-Lip, with MB, with or without US application ($n = 5$). $p < .005$ by students unpaired two tailed t-test. Error bars represent standard deviation. Y axis on D represents % of 6.3 MBq loaded within the HEGF-lip of C. (For interpretation of the references to color in this figure legend, the reader is referred to the web version of this article.)

In both cases the volume of the injectate was 100 μL, with equal mass amounts of HEGF administered which was determined using HPLC. Mice were euthanised at 24 h. Xenografts and organs were harvested, weighed and the amount of radioactivity counted using a HIDEX automatic gamma counter (HIDEX, Lemminkäisenkatu 62 FIN-20520 Turku, Finland).

2.1.14. Blood circulation time

SCID mice (3 per group) were anaesthetised and received either [^{111}In]In-HEGF-Lip (6 MBq) or [^{111}In]In-HEGF (6 MBq) i.v. by cannula followed by a saline flush of approximately 20 μL to account for the dead volume in the length of the cannula. Animals were placed in a bespoke mouse cradle fitted to a VECTOR 4 CT scanner (MI-Labs, Heidelberglaan, Utrecht, The Netherlands) and their temperature was maintained at 37 °C using a thermostatic heating plate and monitoring via a rectal probe. Dynamic single photon emission tomography (SPECT) images were acquired (1 frame every 36 s for 2 h) centred on the heart. A CT scan was acquired for anatomical information. See Supplementary Information for more details. Animals were euthanised at the end of the imaging procedure. Images were reconstructed via MI-Labs software and the signal due to [^{111}In]In^{3+} in the heart over time was analysed via PMOD software (PMOD Technologies LLC, Sumatrastrasse 25, CH-8006 Zurich, Switzerland).

2.1.15. Tumour uptake of radioactivity

Tumour uptake was determined at 24 h via organ harvesting as outlined above. For US enhanced delivery this was examined at 20 min via SPECT imaging as outlined above except acquiring 2 frames over 5 min in the area of the tumour and excluding the other areas of the body. The use of this 20 min time point allowed cavitation mediated uptake to be distinguished from EPR mediated uptake which may have been evident at 24 h. The images were quantified in PMOD. The average amount of radioactivity within the tumour or an organ was obtained from mean pixel values within the ROI volume. Assuming a tissue density of 1 g/mL, the ROIs were converted to MBq per gram and were then divided by the total administered activity to obtain the imaging ROI-derived percentage administered activity per gram of tissue (%ID/g).

2.1.16. Focused ultrasound in vivo

Mice (3 per group) received either [^{111}In]In-HEGF-Lip (6 MBq) i.v. followed by SV (50 μL) or [^{111}In]In-HEGF-Lip (6 MBq) followed by SV (50 μL) as well as tumour targeted US. The total injection time for the combined treatment of liposomes and SV was 90 ± 20 s. US (1 MHz, 1 MPa, 30% duty cycle, 10 ms pulse period) was applied to tumours for 5 min. US was applied after injection of SV was completed. Tumours were treated when they reached an approximate volume of 70–100 mm^3. A mouse was placed on an acoustically transparent mylar

bed above a water bath thermostatically controlled at 37 °C. A 1.0 MHz center frequency US source was positioned in the water directly underneath the animal (Supplementary Fig. 3). The focus of the source was aligned to a spot marked on the mylar bed where the target tumour would be placed. The center of the transducer housed a 7.5 MHz US transducer (Panametrics V320-SU-F 1.75PTF, Olympus NDT, Essex, UK) that was used as a passive cavitation detector (PCD). Receiver signals were high-pass filtered (F5081-2P0, Allen Avionics, Mineola, NY, USA), preamplified (SR445A, SRS, Sunnyvale, CA, USA), digitized (Handyscope HS3, TiePie Engineering, Netherlands) and streamed to a laptop computer disk. For analysis of cavitation activity, PCD time series data sets were processed in Matlab (Mathworks, Natick, MA, USA) using Welch's method for power spectrum calculation, implemented with temporal windows of 80 μs (2.5% of typical source drive pulse length) with 50% window overlap. Before therapy was started, a small amount of centrifuged US coupling gel (Aquasonic 100, Parker Laboratories, Fairfield, NJ) was applied to the mylar at the mark where the tumour would be placed. Centrifuging the coupling gel ensured no air bubbles were present.

3. Results and discussion

3.1. Liposome characterisation

Liposome modal diameter, as assessed by DLS (Supplementary Fig. 4A, B), was found to be 175 nm with a polydispersity index of 0.15. Transmission electron microscopy images were in accordance with this size range, with a spherical shaped lipid shell evident, as shown in Fig. 2A. Similar size and polydispersity readings were obtained for all liposome formulations, regardless of the presence or absence of HEGF or [^{111}In]In^{3+} (supplementary Fig. 4C).

3.2. Passive loading of liposomes with HEGF

The level and efficiency of HEGF loading into liposomes and the success of ultracentrifugation and SE centrifugation in removing free non-encapsulated HEGF was assessed using HPLC. 15% of the added HEGF was loaded into the liposomes The dashed red lines in Fig. 2B shows the peak at 18 min that is present in the profile for HEGF alone and the profile for HEGF-Lip but absent for control 'Empty Liposomes' to which no HEGF was added. This level of loading is in-line with that typically achieved by similar passive loading techniques [40]. This resulted in a peptide to lipid ratio of approximately 1:315 mg, considering lipid loss during cleaning. This is a limitation for all passive protein loading techniques which are inefficient because the liposomes cannot entrap 100% of the surrounding protein solution [41]. Cleaning techniques may also result in loss of the lipids. Importantly, the purification method employed in this study does allow the recovery and potential re-use of non-encapsulated HEGF [42]. The quantities of lipid and HEGF combined would be acceptable for human use if scaled-up based on calculations from Barenholz and Vallis *et al.* [11,18].

3.3. Indium-111 labelling of liposomes

Having established that HEGF could be loaded into the liposomes the question of whether the internalised peptide could then be rapidly and efficiently radiolabelled with [^{111}In]In^{3+} was investigated. Fig. 2C shows that of the 11 MBq of [^{111}In]$InCl_3$ added to control empty liposomes (i.e. no HEGF), < 1 MBq was retained after washing. Similarly, when liposomes were loaded with HEGF and [^{111}In]$InCl_3$ added before the non-encapsulated HEGF was removed by purification ('internal and external') the amount of radioactivity (2 MBq) was low (Supplementary Fig. 5). This emphasises the need to remove free HEGF through purification after the passive loading step. In contrast when [^{111}In]$InCl_3$ was added to purified HEGF liposomes > 6 MBq (57% ± 10) of the [^{111}In]In^{3+} was encapsulated. Furthermore, > 75% of the [^{111}In]In^{3+} remained incorporated after the liposomes were added to serum at 37 °C for 5.5 h (Supplementary Fig. 5D). When these purified products were analysed by SG-ITLC (Supplementary Fig. 6) it was apparent that of the 1 MBq associated with the empty liposomes, 34% was incorporated. This radiolabelling is possible because [^{111}In]$InCl_3$ can pass passively through the lipid shell, however, in the absence of HEGF, there is no mechanism to retain [^{111}In]$InCl_3$ inside the liposome and so over time it can diffuse back out. In contrast, of the 6 MBq associated with HEGF-DTPA liposomes 93% remained at the SG-ITLC origin demonstrating efficient and robust incorporation within the liposomes.

To probe the nature of the [^{111}In]In^{3+} association with empty liposomes further, Triton X 100 was added to the empty liposomes and SG-ITLC analysis repeated (Supplementary Fig. 7). Notably, post-Triton addition, 15% of the 1 MBq still remained at the origin. This suggests that a low level of [^{111}In]$InCl_3$ interacts with the liposomal surface but is not internalised or retained. It is possible that this observation results from a transient interaction between the phosphate groups on the phospholipids of the liposome and the [^{111}In]$InCl_3$ [43].

3.4. Ultrasound stimulated release

[^{111}In]In-HEGF-Lip were tested for US enhanced release in the presence of cavitating MBs. The amount [^{111}In]In-HEGF that was released from liposomes that were exposed to MBs and US (i.e. cavitation) for 20 s was 12 ± 4% of the total. In contrast, in the absence of cavitation only 1.5 ± 2% of the cargo was released, as shown in Fig. 2D. Graham *et al.* reported 20–30% release of doxorubicin from liposomes using a similar setup. Lentacker *et al.* reported 'significant' release of doxorubicin from liposomes attached to MBs and this resulted in a doubling of cell kill relative to liposomes that were not exposed to US [14,44]. However, these examples may not be directly relevant as they concern the release of a drug (doxorubicin) with a much lower molecular weight than [^{111}In]In-HEGF. The release of 12 ± 4% of [^{111}In]In-HEGF would be interesting to examine clinically in terms of the added cost of ultrasound relative to improvements in patient treatment to [^{111}In]In-HEGF-Lip alone. Attachment of [^{111}In]In-HEGF-Lip to MBs could improve release and therapeutic efficacy [45] but would also add complexity to the manufacture and purification process perhaps precluding facile synthesis in a hospital setting. Cavitation caused release of [^{111}In]In-HEGF from the liposomes *in vitro*, but *in vivo* the ultrasound would also cause enhanced delivery [36] and improved endothelial opening [46] the combination of which is likely improve cost-to-benefit. It is important to note that whilst the *in vitro* experiments were limited to a 20 s ultrasound exposure time, *in vivo* experiments allow for replenishment of MBs and so longer exposure times on the order of minutes can occur. With regard to safety, recent research has shown that the observed extent of cavitation would have minimal impact on red blood cells [47].

3.5. Cellular uptake

Cellular uptake of [^{111}In]In-HEGF-Lip with and without US was measured after incubation of both cell lines for 2 h. A difference in uptake was noted to be dependent on US application, and not on receptor availability (Fig. 3A). Incubation of MDA-MB-468 cells with [^{111}In]In-HEGF-Lip, MBs and exposure to US gave an increase in CPM/mg of protein relative to cells exposed to [^{111}In]In-HEGF-Lip and MBs but no US. The same finding was evident with MCF7 cells which have low expression of EGFR. No statistical difference between the uptake into the two cell lines when exposed to US was observed ($P > .05$). To exclude the possibility that interaction between MB cavitation and liposomes could be the cause of non-specific association with both cell lines, their exposure to liposomes and to cavitation events were temporally separated. Cells were incubated with [^{111}In]In-HEGF-Lip, and a media change and wash performed after 2 h, followed by addition of

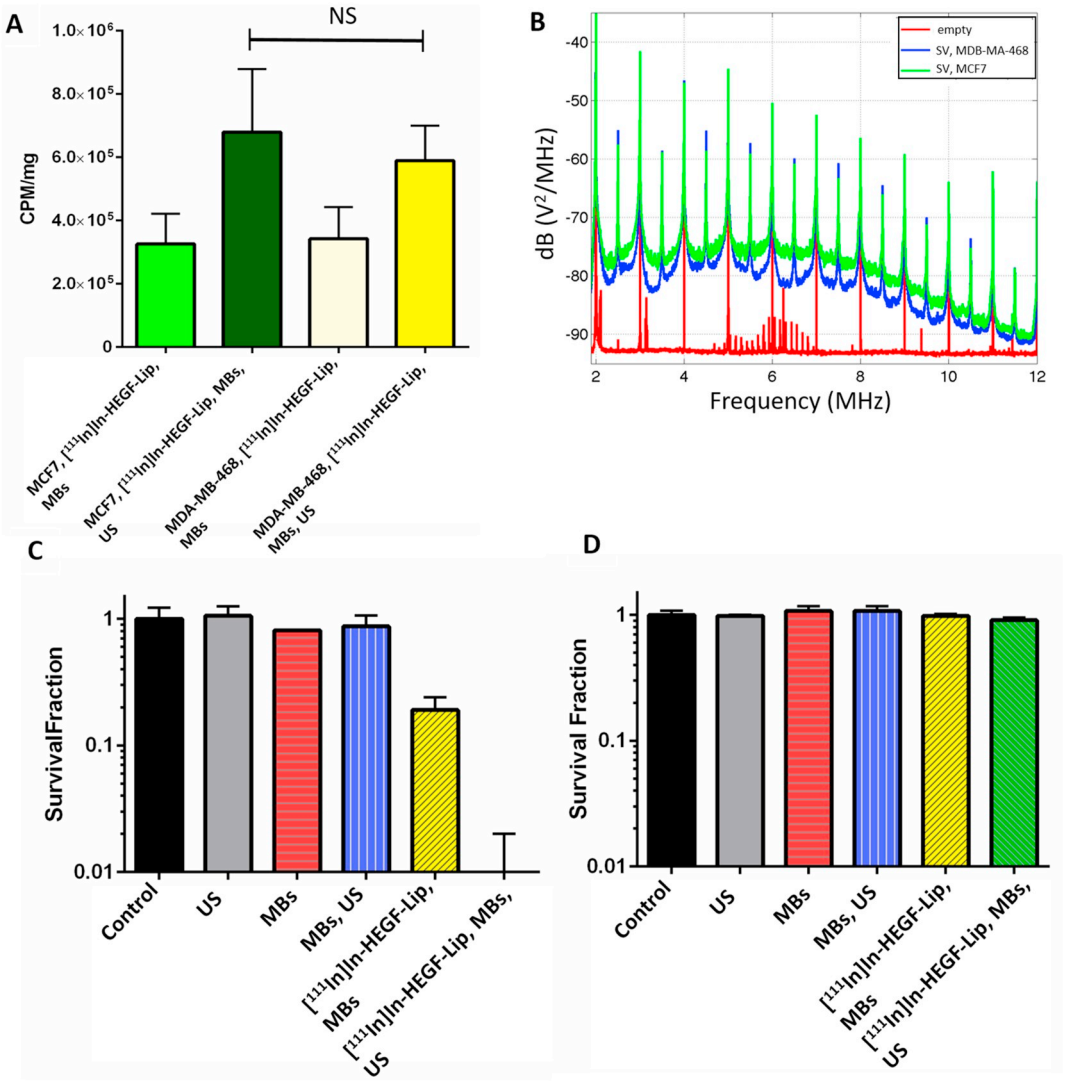

Fig. 3. Assessing delivery of [^{111}In]In-HEGF to cells *in vitro*. A) Counts per minute (CPM) per mg of protein for MCF7 cells and MDA-MB-468 cells exposed to [^{111}In]In-HEGF-Lip and MBs with and without US for 20 s, followed by incubation for 2 h ($n = 3$; $p > .05$; two tailed student's t-test). B) Examples of PCD power spectra averaged over the 20-s US exposure period for an empty dish (control containing only media and no cells) and two cell lines with SV and [^{111}In]In-HEGF-Lip. Relative to the control, the latter two spectra show elevated responses at integer and half-integer multiples of the drive frequency (1.0 MHz) indicating nonlinear bubble vibration, along with broadband elevation at all frequencies, suggesting bubble collapse. C) Comparison of colony survival for MDA-MB-468 cells; controls, cells exposed to US only, MBs only, MBs and US, [^{111}In]In-HEGF-Lip and MBs, [^{111}In]In-HEGF-Lip and MBs and US. D) Comparison of MCF7 cells following exactly the same exposure conditions ($n = 3$).

MBs with or without US application. No difference in uptake was then observed with and without US (Supplementary Fig. 8A and B). The results indicate that the US is not only causing release of [^{111}In]In-HEGF as shown in Fig. 2D but also potentially driving [^{111}In]In-HEGF-Lip and released [^{111}In]In-HEGF through the cell membrane into the cell cytoplasm regardless of cell EGFR density [48]. This is in accordance with a 'sonoporation' effect reported previously in several *in vitro* experiments [49–51]. To explore this further cell compartments were examined after 24 h (Supplementary Fig. 9C) and showed that the signal for MDA-MB-468 cells was detected in the cytoplasm and the nucleus, whereas for MCF7 there is negligible signal detected in both fractions indicating the sonoporation has a transient effect for MCF7. There is also reduced exposure on the cell membrane. This agrees with mechanism of cytotoxicity for [^{111}In]In-HEGF as reported by Reilly *et al.* which exploits the normal internalisation pathway for peptide growth factors after their binding to cell surface receptors [6]. This pathway involves internalisation of growth factors and their receptors into cytoplasmic vesicles for proteolytic degradation and potential nuclear translocation [52]. The ultrasound causes liposomal release and increased uptake into cells regardless of cell receptor density, but for [^{111}In]In-HEGF to have a cyctotoxic impact it requires the pathway to nuclear transcription. This could possibly require a re-entry mechanism of [^{111}In]In-HEGF and requires further exploration for the impact of ultrasound and nanoparticles on cellular uptake and cytotoxicity.

3.6. Cell survival

Using clonogenic assays it was shown that in the absence of [^{111}In]In-HEGF-Lip the physical stimulus of US and addition of MBs, either alone or in combination, had minimal impact on cell survival in either cell line as the survival fraction (SF) was > 85%. In contrast, [^{111}In]In-HEGF-Lip were highly cytotoxic to MDA-MB-468 cells when used in combination with MBs and US. Whereas SF was maintained at 1 for all conditions in MCF7 cells SF was approximately 100-fold lower in MDA-MB-468 cells exposed to MB plus [^{111}In]In-HEGF-Lip with US. (Fig. 3C and D). Cavitation events triggered by MBs in the presence of US (Fig. 3B) may cause release of [^{111}In]In-HEGF from liposomes allowing receptor mediated uptake to take place. The *in vitro* data shown here

and previous studies by Graham *et al.* [14] indicate that uptake of released payload is likely to be occurring. However, the work of Lentacker *et al.* [49] demonstrates that passage of the whole liposomes into cells is also a possibility. However, MBs with [^{111}In]In-HEGF-lip and US only reduced the viability of EGFR overexpressing cells without impacting cells with minimal EGFR expression (Fig. 3C and D).

Exposure of MDA-MB-468 cells to [^{111}In]In-HEGF-Lip and MBs resulted in 80 ± 5% cell death even in the absence of US. One possible explanation for this observation is that liposome degradation of the liposomes occurred during the 24 h incubation at 37 °C, with release of [^{111}In]In-HEGF which only impacted MDA-MB-468 cells owing to higher EGFR expression.

Cavitation only occurred when MBs were present in solution at the time that US was applied (Fig. 3B). No difference in toxicity was observed between MDA-MB-468 cells and MCF7 cells when MBs were cavitated in the presence of US but absence of [^{111}In]In-HEGF-Lip (Fig. 3C and D). The cavitation signal was highest during the first 1.5 s after which the cavitation signal markedly reduced by a factor of 4–6 and by an order of magnitude after 20 s (Supplementary Fig. 9). It is possible that 20 s of US exposure is longer than required in this *in vitro* set-up.

3.7. In vivo biodistribution

The [^{111}In]In-HEGF-Lip were tested *in vivo* to examine biodistribution and pharmacokinetics. [^{111}In]In-HEGF-Lip was shown to have an extended blood circulation time relative to [^{111}In]In-HEGF. As shown in Fig. 4A the amount of [^{111}In]In-HEGF decreased rapidly to 0.1 ± 0.1% ID/g within thirty minutes, whereas after 2 h, 10 ± 5%ID/g of liposomes were still present in the blood. However, the profile for the liposomes shows a rapid decrease over the course of the first ten minutes post injection (p.i.). The decay for [^{111}In]In-HEGF was exponential with a blood half-life of 174 s ± 19 s. The blood half-life for the [^{111}In]In-HEGF-Lip was bi-exponential with a rapid phase, 101 s ± 61 s, followed by a slower phase ~ 50 min ± 19 min. This is likely to represent a distribution phase followed by an elimination phase [53] but it may also be the consequence of release of up to 25% of the payload due to temperature and serum mediated destabilization (Supplementary Fig. 5), or also possibly due to a small quantity of free [^{111}In]In-HEGF which was not removed during the cleaning process. Notably, after 24 h [^{111}In]In-HEGF-Lip is still detectable in the blood whereas [^{111}In]In-HEGF is below detectable limits (Fig. 4D).

[^{111}In]In-HEGF-Lip results in a change in the 24 h biodistribution that differs from that of [^{111}In]In-HEGF. As shown in Fig. 4B the majority of [^{111}In]In-HEGF accumulated in the kidneys and liver whereas for the liposomal formulation (Fig. 4C) renal clearance reduced by half. Interestingly there is no increased signal in the liver for this liposomal construct, which was unexpected and different to other clinically available liposome formulations [53]. The biodistribution was also confirmed by 24 h SPECT images where signal for [^{111}In]In-HEGF and [^{111}In]In-HEGF-Lip is detectable in the kidneys and the liver (Supplementary Fig. 10). Using scintillation counting of organs *ex vivo*, most organs have double the amount of accumulated [^{111}In]In^{3+} when the liposomal formulation was used relative to the free radiopeptide. This effect was also evident in the tumour as the liposomal formulation delivered over twice the amount (2.2 ± 0.5%ID/g) relative to [^{111}In]In-HEGF (0.8 ± 0.2%ID/g) as shown in Fig. 4E. The tumour to blood ratio was 1.77 for [^{111}In]In-HEGF-Lip 24 h after injection, however, no ratio could be calculated for the ^{111}In-HEGF because the quantity in the blood was negligible. The tumour to muscle ratio was 3.15 ± 1.8 for the [^{111}In]In-HEGF-Lip and 5.69 ± 2.4 for [^{111}In]In-HEGF 24 h after injection but, these figures were not statistically different, indicating that [^{111}In]In-HEGF-Lip is distributed more widely throughout the organs resulting in a higher background level. For [^{111}In]In-HEGF-Lip at 24 h approximately 1%ID/g remains in the blood and approximately 2%ID/g is recovered from the tumour. There is a possibility that the blood load may over-estimate the level being assigned to tumour accumulation. However, it should be noted that the tumours are very poorly perfused (Supplementary Fig. 11) and blood quantity in the tumour may be negligible. This is evidenced by the fact that at 20 min (when blood activity levels were 15 × higher than at 24 h) the tumour associated level without ultrasound (Fig. 5A) was only 0.9 ± 0.4%ID/g. However, the extended circulation time and the change in biodistribution are strikingly different for [^{111}In]In-HEGF-Lip relative to [^{111}In]In-HEGF alone. Further investigation of the role of the RES in the capture, degradation and excretion of the liposomes would be useful in understanding and optimising the PK of this formulation to allow further enhancements of passive and potentially active delivery to tumours.

The ~20% uptake in the kidneys from [^{111}In]In-HEGF-Lip (Fig. 5C) was unexpected even though it represents only half the amount observed for [^{111}In]In-HEGF. One possible explanation is slow release of the [^{111}In]In-HEGF from inside the liposome over time. Another possibility is release of [^{111}In]In-HEGF bound to the liposome surface over time. However, this is less likely because the liposomes are PEGylated and as such there are no potential binding sites for HEGF. Furthermore, the pharmacokinetic profile and biodistribution of the liposomes did not match those produced by a liposome formulation with externally bound [^{111}In]In-HEGF [54] and there was no correlation of *in vitro* cellular uptake of [^{111}In]In-HEGF-Lip and EGFR density (Fig. 3A) which would be expected of liposomes with surface bound [^{111}In]In-HEGF.

3.8. Ultrasound enhanced delivery

Having established that the [^{111}In]In-HEGF-Lip formulation provided more a favourable PK compared to [^{111}In]In-HEGF, the impact of tumour directed US exposure on the liposomes was studied. Intravenous [^{111}In]In-HEGF-Lip and MB delivery to tumour (20 min p.i.) with the application of US was 2.1 ± 0.5%ID/g versus 0.9 ± 0.4%ID/g for [^{111}In]In-HEGF-Lip and MBs alone ($n = 3$, $P < .05$). Cavitation was confirmed via PCD data (Fig. 5B) specifically in the appearance of ultraharmonics (half integer multiples of the FUS frequency) and broadband noise which are well-known characteristics of nonlinear bubble behaviour in an US field [55]. In all US experiments with MBs, the total (ultraharmonic + broadband) cavitation level was at least five times greater than the root mean square background noise. Such acoustic feedback provides confidence that cavitation events occurred within the tumour at the time of liposome transition through the tumour vasculature. SPECT images of mice tumours taken at 20 min (Fig. 5C and D) are consistent with enhanced tumour delivery, since signal intensity in the area of the tumour was greater following application of US compared to omission of US. Signal was noted immediately beyond the tumour, indicating that the area of US exposure was potentially more extensive than necessary. However, the clearly enhanced uptake observed in Fig. 5 A and C versus D, does suggest that specific triggered release/delivery of a radiopharmaceutical from a liposomal carrier can be achieved *in vivo*. These results are in accordance with a previous report of delivery of a PET integrin tracer incorporated within a microbubble where focused US doubled tumour accumulation within 15 min in a human glioblastoma xenograft [56]. This result is likely a combination of liposome opening [14], enhanced delivery [36] and potential opening of the endothelial barrier [46], however which mechanism is dominant requires further investigation.

Notably, it is apparent that [^{111}In]In-HEGF-Lip can also achieve similar (~2%ID/g) tumour accumulation via simple passive means after 24 h (Fig. 4E). In previous studies US has been shown to enhance the delivery of PLGA nanoparticles carrying microRNA miR-122 by 4–14 fold in human colon cancer xenografts in mice [57]. The reason for the lower increase reported here relative to this previous work is likely due to the poor vascularity of the tumour model and lack of penetration of MBs and [^{111}In]In-HEGF-Lip to the tumour core. In Fig. 5E and F autoradiography of the tumour sections show that

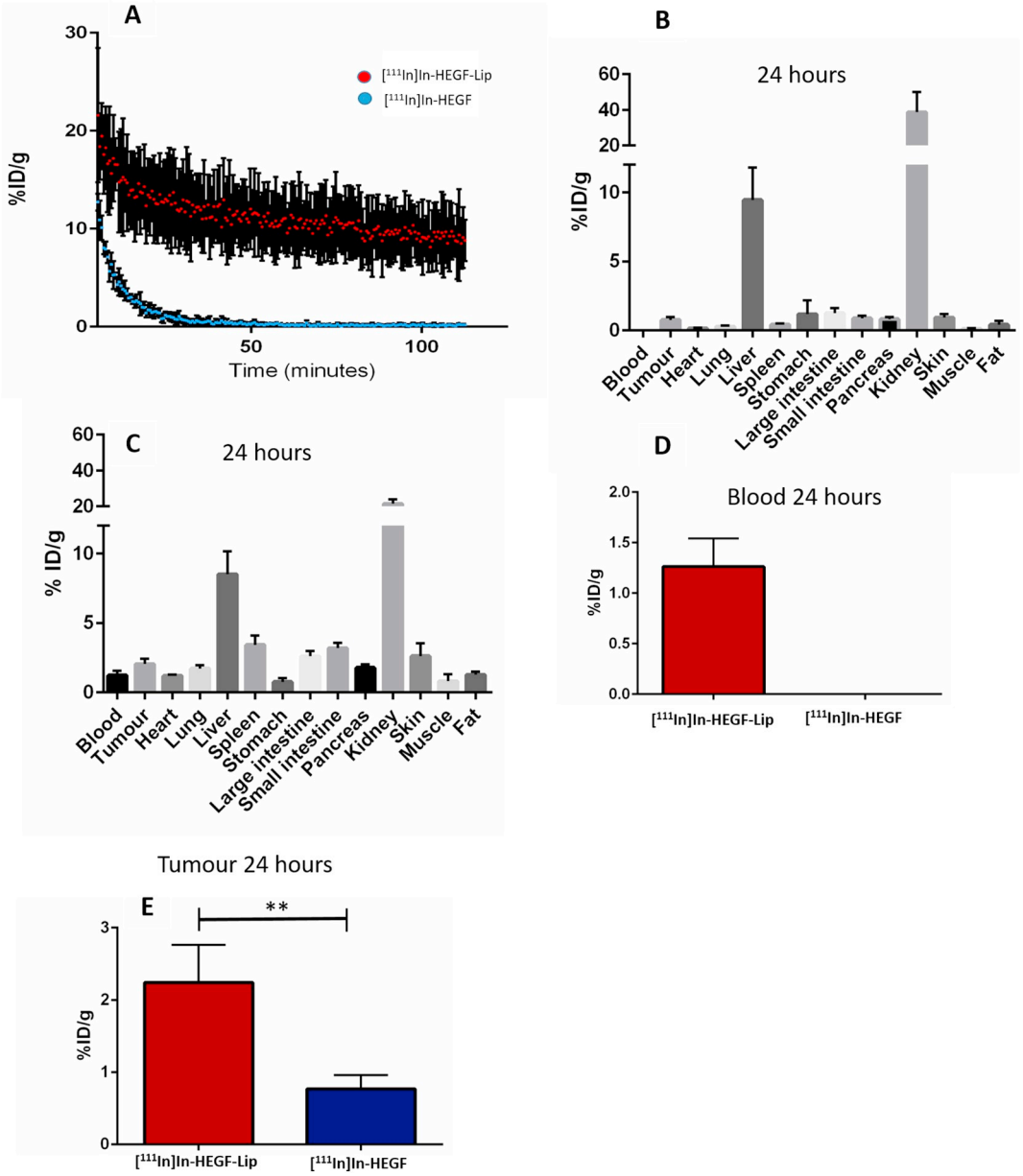

Fig. 4. Distribution and pharmacokinetics in a murine xenograft model in percentage of injected dose per gram (%ID/g), A) blood lifetime of [^{111}In]In-HEGF-Lip (red) and [^{111}In]In-HEGF (blue) over 2 h from SPECT imaging ($n = 3$), B) Biodistribution of [^{111}In]In-HEGF ($n = 4$) and C) [^{111}In]In-HEGF-Lip ($n = 4$) 24 h post injection, D) levels of radioactivity in the blood at 24 h from scintillation counting. ($n = 4$) standard deviation shown, and E) Tumour uptake at 24 h with unpaired student t-test, ** = $p < .005$.

although US-mediated cavitation increased the amount of liposomes deposited in the treated peripheral 'ring' of the tumour, the core has a low signal intensity regardless of the addition of US, indicating poor delivery beyond this perfused ring. There was no statistical difference in the penetration depth of liposomes with and without US. Contrast enhanced imaging also showed a low acoustic signal intensity within the tumour core (Fig. 5G). The vascularity of the tumours was further examined via MRI and contrast enhanced US and compared with other tumour models (Supplementary Fig. 11). The results showed that the MDA-MB-468 tumours are very poorly vascularised relative to a CT26 tumour model, which has been previously used for US enhanced delivery [58]. However, the CT26 tumour cell line is of murine origin and does not overexpress EGFR, making it an unsuitable model for our studies.

If the MBs cannot enter the tumour environment then it will not be possible for them to cavitate and enhance delivery and release of the [^{111}In]In-HEGF-Lip. However, it is notable that even in a poorly vascularised tumour, MDA-MB-468, the application of US had a statistically significant impact on delivery, which might indicate therapeutic potential even for poorly vascularised tumours and requires further investigation. However, this outcome provides an important point to examine the vasculature of the tumour line chosen in conjunction with a molecular target for enhancing delivery via US. Whether using this US approach to achieve rapid delivery of high peak intra-tumour concentration is therapeutically preferable to the slow prolonged delivery achieved by the EPR effect also requires further investigation. It is also possible cavitation within the tumour could also have an impact upon the vasculature causing potential changes and impacting repeat treatments. As such investigating tumour vasculature before and after treatment would be recommended in the future.

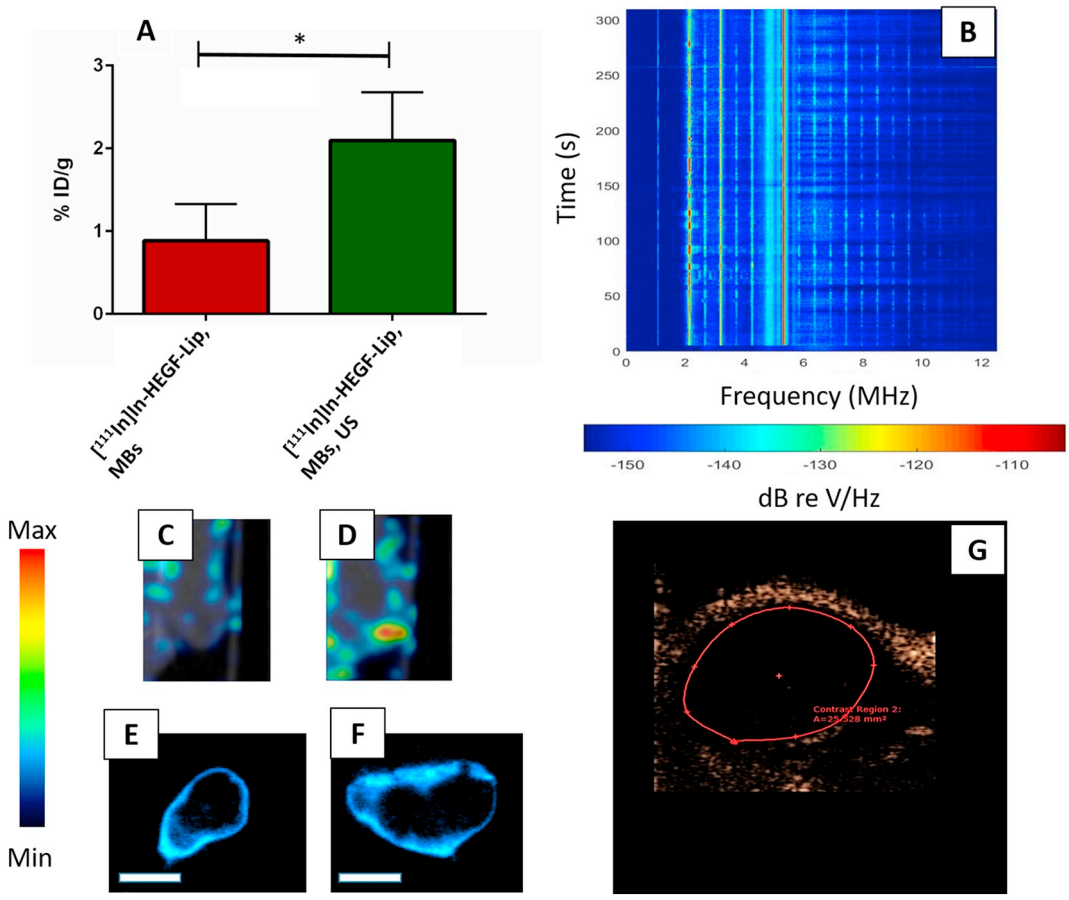

Fig. 5. US enhanced tumour uptake of [^{111}In]In-HEGF-Lip. A) Tumour uptake 20 min after injection of [^{111}In]In-HEGF-Lip, MBs comparing US to non-US treated tumours, unpaired student t-test $p < .05$, $n = 3$, error bars represent standard deviations. B) Acoustic data collected during treatment providing validation of cavitation occurrence. C) Representative SPECT images of mouse tumour area after injection of [^{111}In]In-HEGF-Lip without US and D) with US. E) Autoradiography after 24 h examining distribution of indium within a tumour section following treatment with [^{111}In]In-HEGF-Lip and MBs or F) [^{111}In]In-HEGF-Lip and MBs and US (scale bar: 3 mm), G) contrast enhanced US image of a MDA-MB-468 tumour in an athymic nude mouse with MBs.

4. Conclusion

This exploratory research has shown that radiopharmaceutical loaded nanoparticles combined with cavitation enhanced delivery does have clinical potential. Each stage requires optimisation and further investigation but the current strategy is relevant for radiopharmacies, only impacts cells overexpressing EGFR, has extended the circulation time, changed the biodistribution and increased tumour uptake warranting further study. This research also highlights potential pitfalls such as the impact of vasculature on US enhanced delivery which is another key variable for tumour target selection along with target receptor/antigen presentation.

5. Limitations

As this research combined existing technologies minimal characterisation was performed for the nanoparticles and the radiotherapeutic which have been examined in previous publications. Further characterisation/optimisation of the loading techniques and the nanoparticles will be required before progressing to other experiments. Notably optimising radiolabelling to remove the SE centrifugation, which will not be desirable in a radiopharmacy. Use of physical stimuli to deliver therapeutics must overcome physical barriers in the human body. Xenograft tumours in a mouse model are likely to be different morphologically from human tumours and certainly in terms of access for US. Development of *ex vivo* models replicating physical conditions found within the human body may be a means to more accurately assess US enhanced delivery of radiopharmaceuticals for a clinical setting. Further improvements in cavitation assisted delivery may potentially be realised through optimisation of US exposure conditions paired with model-specific perfusion analysis. Improved matching of the pharmacokinetics of the liposomes with agents used to seed cavitation may help sustain and improve the delivery over longer periods, i.e. the replacement of MBs with polymeric nanocups described by Myers *et al.* [59], a formulation which nucleates cavitation over an extended period.

Acknowledgements

This work was supported by the Engineering and Physical Sciences Research Council (EPSRC) OXCD3 Grant EP/L024012. The authors would like to thank James Fisk and David Salisbury for their contribution to the design and construction of the equipment. The authors would also like to thank Dr. Veerle Kersemans and Dr. Sean Smart for help and advice with imaging and analysis. The authors also acknowledge Dr. Mary-Ann Xavier for her scientific advice.

Appendix A. Supplementary data

Supplementary information to this article can be found online at https://doi.org/10.1016/j.jconrel.2019.12.045. Raw data are available from the University of Oxford ORA data repository (https://ora.ox.ac.uk/objects/uuid:8764400c-27dc-4f3e-990a-d21dbeb0812b).

References

[1] M.R. Gill, N. Falzone, Y. Du, K.A. Vallis, Targeted radionuclide therapy in combined-modality regimens, Lancet Oncol. 18 (2017) e414–e423.
[2] J. Strosberg, G. El-Haddad, E. Wolin, A. Hendifar, J. Yao, B. Chasen, E. Mittra, P.L. Kunz, M.H. Kulke, H. Jacene, D. Bushnell, T.M. O'Dorisio, R.P. Baum, H.R. Kulkarni, M. Caplin, R. Lebtahi, T. Hobday, E. Delpassand, E. Van Cutsem, A. Benson, R. Srirajaskanthan, M. Pavel, J. Mora, J. Berlin, E. Grande, N. Reed, E. Seregni, K. Öberg, M. Lopera Sierra, P. Santoro, T. Thevenet, J.L. Erion, P. Ruszniewski, D. Kwekkeboom, E. Krenning, Phase 3 trial of 177Lu-dotatate for midgut neuroendocrine tumors, N. Engl. J. Med. 376 (2017) 125–135.
[3] M. Boegemann, A.J. Schrader, K. Rahbar, 177Lu-PSMA-Therapie, Der Urologe 56 (2017) 1440–1444.
[4] B. Cornelissen, K. A. Vallis, Targeting the nucleus: an overview of auger-electron radionuclide therapy, Curr. Drug Discov. Technol. 7 (2010).
[5] J.V. Leyton, M.D. Hu, C. Gao, P.V. Turner, J.E. Dick, M. Minden, R.M. Reilly, Auger electron radioimmunotherapeutic agent specific for the CD123(+)/CD131(−) phenotype of the Leukemia stem cell population, J. Nucl. Med. 52 (2011) 1465–1473.
[6] R.M. Reilly, P. Chen, J. Wang, D. Scollard, R. Cameron, K.A. Vallis, Preclinical pharmacokinetic, biodistribution, toxicology, and dosimetry studies of in-111-DTPA-human epidermal growth factor: an auger electron-emitting radiotherapeutic agent for epidermal growth factor receptor-positive breast cancer, J. Nucl. Med. 47 (2006) 1023–1031.
[7] P. Lai, W. Daear, R. Löbenberg, E.J. Prenner, Overview of the preparation of organic polymeric nanoparticles for drug delivery based on gelatine, chitosan, poly(d,l-lactide-co-glycolic acid) and polyalkylcyanoacrylate, Colloids Surf. B: Biointerfaces 118 (2014) 154–163.
[8] A.Z. Wang, K. Yuet, L.F. Zhang, F.X. Gu, M. Huynh-Le, A.F. Radovic-Moreno, P.W. Kantoff, N.H. Bander, R. Langer, O.C. Farokhzad, ChemoRad nanopartides: a novel multifunctional nanoparticle platform for targeted delivery of concurrent chemoradiation, Nanomedicine 5 (2010) 361–368.
[9] E. Vegt, M. Melis, A. Eek, M. de Visser, M. Brom, W.J.G. Oyen, M. Gotthardt, M. de Jong, O.C. Boerman, Renal uptake of different radiolabelled peptides is mediated by megalin: SPECT and biodistribution studies in megalin-deficient mice, Eur. J. Nucl. Med. Mol. Imaging 38 (2011) 623–632.
[10] L. Song, N. Falzone, K.A. Vallis, EGF-coated gold nanoparticles provide an efficient nano-scale delivery system for the molecular radiotherapy of EGFR-positive cancer, Int. J. Radiat. Biol. 92 (2016) 716–723.
[11] K.A. Vallis, R.M. Reilly, D. Scollard, P. Merante, A. Brade, S. Velauthapillai, C. Caldwell, I. Chan, M. Freeman, G. Lockwood, N.A. Miller, B. Cornelissen, J. Petronis, K. Sabate, Phase I trial to evaluate the tumor and normal tissue uptake, radiation dosimetry and safety of (111)in-DTPA-human epidermal growth factor in patients with metastatic EGFR-positive breast cancer, Am. J. Nuclear Med. Mol. Imag. 4 (2014) 181–192.
[12] G. Milano, J.P. Spano, B. Leyland-Jones, EGFR-targeting drugs in combination with cytotoxic agents: from bench to bedside, a contrasted reality, Br. J. Cancer 99 (2008) 1–5.
[13] F. Danhier, O. Feron, V. Préat, To exploit the tumor microenvironment: passive and active tumor targeting of nanocarriers for anti-cancer drug delivery, J. Control. Release 148 (2010) 135–146.
[14] S.M. Graham, R. Carlisle, J.J. Choi, M. Stevenson, A.R. Shah, R.S. Myers, K. Fisher, M.-B. Peregrino, L. Seymour, C.C. Coussios, Inertial cavitation to non-invasively trigger and monitor intratumoral release of drug from intravenously delivered liposomes, J. Control. Release 178 (2014) 101–107.
[15] S.D. Li, L. Huang, Pharmacokinetics and biodistribution of nanoparticles, Mol. Pharm. 5 (2008) 496–504.
[16] H. Maeda, J. Wu, T. Sawa, Y. Matsumura, K. Hori, Tumor vascular permeability and the EPR effect in macromolecular therapeutics: A review, J. Control. Release 65 (2000) 271–284.
[17] S. Wilhelm, A.J. Tavares, Q. Dai, S. Ohta, J. Audet, H.F. Dvorak, W.C.W. Chan, Analysis of nanoparticle delivery to tumours, Nat. Rev. Mater. 1 (2016) 16014.
[18] Y. Barenholz, Doxil® - the first FDA-approved nano-drug: lessons learned, J. Control. Release 160 (2012) 117–134.
[19] T.M. Allen, P.R. Cullis, Liposomal drug delivery systems: from concept to clinical applications, Adv. Drug Deliv. Rev. 65 (2013) 36–48.
[20] D. Papahadjopoulos, T.M. Allen, A. Gabizon, E. Mayhew, K. Matthay, S.K. Huang, K.D. Lee, M.C. Woodle, D.D. Lasic, C. Redemann, F.J. Martin, Sterically stabilized liposomes: improvements in pharmacokinetics and antitumor therapeutic efficacy, Proc. Natl. Acad. Sci. U. S. A. 88 (1991) 11460–11464.
[21] L.D. Mayer, M.B. Bally, P.R. Cullis, Uptake of adriamycin into large unilamellar vesicles in response to a pH gradient, Biochim. Biophys. Acta Biomembr. 857 (1986) 123–126.
[22] U. Pick, Liposomes with a large trapping capacity prepared by freezing and thawing of sonicated phospholipid mixtures, Arch. Biochem. Biophys. 212 (1981) 186–194.
[23] O.C. Boerman, G. Storm, W.J.G. Oyen, L. Van Bloois, J.W.M. Van der Meer, R.A.M.J. Claessens, D.J.A. Crommelin, F.H.M. Corstens, Sterically stabilized liposomes labeled with Indium-111 to image focal infection, J. Nucl. Med. 36 (1995) 1639–1644.
[24] M.R. Lewis, R. Kannan, Development and applications of radioactive nanoparticles for imaging of biological systems, Wiley Interdisc. Rev. 6 (2014) 628–640.
[25] P.L. Beaumier, K.J. Hwang, An efficient method for loading Indium-111 into liposomes using acetylacetone, J. Nucl. Med. 23 (1982) 810–815.
[26] K.J. Hwang, J.E. Merriam, P.L. Beaumier, K.F.S. Luk, Encapsulation, with high efficiency, of radioactive metal ions in liposomes, BBA - Gen. Subj. 716 (1982) 101–109.
[27] L.D.G. Mota, A.L.B. De Barros, L.L. Fuscaldi, M.C. De Oliveira, V.N. Cardoso, Long-circulating and pH-sensitive liposome preparation trapping a radiotracer for inflammation site detection, J. Nanosci. Nanotechnol. 15 (2015) 4149–4158.
[28] B. Goins, R. Klipper, A.S. Rudolph, R.O. Cliff, R. Blumhardt, W.T. Phillips, Biodistribution and imaging studies of technetium-99m-labeled liposomes in rats with focal infection, J. Nucl. Med. 34 (1993) 2160–2168.
[29] T.H. Chow, Y.Y. Lin, J.J. Hwang, H.E. Wang, Y.L. Tseng, V.F. Pang, S.J. Wang, J. Whang-Peng, G. Ting, Diagnostic and therapeutic evaluation of 111In-vinorelbine-liposomes in a human colorectal carcinoma HT-29/luc-bearing animal model, Nucl. Med. Biol. 35 (2008) 623–634.
[30] D.S. Ferreira, F.A. Boratto, V.N. Cardoso, R. Serakides, S.O. Fernandes, L.A.M. Ferreira, M.C. Oliveira, Alendronate-coated long-circulating liposomes containing 99mtechnetium-ceftizoxime used to identify osteomyelitis, Int. J. Nanomedicine 10 (2015) 2441–2450.
[31] A.I. Jensen, G.W. Severin, A.E. Hansen, F.P. Fliedner, R. Eliasen, L. Parhamifar, A. Kjær, T.L. Andresen, J.R. Henriksen, Remote-loading of liposomes with manganese-52 and in vivo evaluation of the stabilities of 52Mn-DOTA and 64Cu-DOTA using radiolabelled liposomes and PET imaging, J. Control. Release 269 (2018) 100–109.
[32] J.R. Henriksen, A.L. Petersen, A.E. Hansen, C.G. Frankær, P. Harris, D.R. Elema, A.T. Kristensen, A. Kjær, T.L. Andresen, Remote loading of 64Cu2+ into liposomes without the use of ion transport enhancers, ACS Appl. Mater. Interfaces 7 (2015) 22796–22806.
[33] M. Rotman, M.M. Welling, A. Bunschoten, M.E. de Backer, J. Rip, R.J.A. Nabuurs, P.J. Gaillard, M.A. van Buchem, S.M. van der Maarel, L. van der Weerd, Enhanced glutathione PEGylated liposomal brain delivery of an anti-amyloid single domain antibody fragment in a mouse model for Alzheimer's disease, J. Control. Release 203 (2015) 40–50.
[34] S. Sofou, B.J. Kappel, J.S. Jaggi, M.R. McDevitt, D.A. Scheinberg, G. Sgouros, Enhanced retention of the α-particle-emitting daughters of actinium-225 by liposome carriers, Bioconjug. Chem. 18 (2007) 2061–2067.
[35] E. Quaia, Contrast Media in Ultrasonography, (2005).
[36] R. Carlisle, J. Choi, M. Bazan-Peregrino, R. Laga, V. Subr, L. Kostka, K. Ulbrich, C.C. Coussios, L.W. Seymour, Enhanced tumor uptake and penetration of virotherapy using polymer stealthing and focused ultrasound, J. Natl. Cancer Inst. 105 (2013) 1701–1710.
[37] R. Myers, M. Grundy, C. Rowe, C.M. Coviello, L. Bau, P. Erbs, J. Foloppe, J.-M. Balloul, C. Story, C.C. Coussios, R. Carlisle, Ultrasound-mediated cavitation does not decrease the activity of small molecule, antibody or viral-based medicines, Int. J. Nanomedicine 13 (2018) 337–349.
[38] R.M. Reilly, J. Gariépy, Factors influencing the sensitivity of tumor imaging with a receptor-binding radiopharmaceutical, J. Nucl. Med. 39 (1998) 1036–1043.
[39] M. Maji, S. Mazumder, S. Bhattacharya, S.T. Choudhury, A. Sabur, M. Shadab, P. Bhattacharya, N. Ali, A lipid based antigen delivery system efficiently facilitates MHC class-I antigen presentation in dendritic cells to stimulate CD8(+) T cells, Sci. Rep. 6 (2016) (27206–27206).
[40] J.-P. Colletier, B. Chaize, M. Winterhalter, D. Fournier, Protein encapsulation in liposomes: efficiency depends on interactions between protein and phospholipid bilayer, BMC Biotechnol. 2 (2002) (9–9).
[41] A. Akbarzadeh, R. Rezaei-Sadabady, S. Davaran, S.W. Joo, N. Zarghami, Y. Hanifehpour, M. Samiei, M. Kouhi, K. Nejati-Koshki, Liposome: classification, preparation, and applications, Nanoscale Res. Lett. 8 (2013) (102–102).
[42] J.C. Giddings, F.J. Yang, M.N. Myers, Flow field-flow fractionation as a methodology for protein separation and characterization, Anal. Biochem. 81 (1977) 395–407.
[43] R.E. Weiner, Role of phosphate-containing compounds in the transfer of Indium-111 and Gallium-67 from transferrin to ferritin, J. Nucl. Med. 30 (1989) 70–79.
[44] I. Lentacker, B. Geers, J. Demeester, S.C. De Smedt, N.N. Sanders, Design and evaluation of doxorubicin-containing microbubbles for ultrasound-triggered doxorubicin delivery: cytotoxicity and mechanisms involved, Mol. Ther. 18 (2010) 101–108.
[45] B. Geers, I. Lentacker, N.N. Sanders, J. Demeester, S. Meairs, S.C. De Smedt, Self-assembled liposome-loaded microbubbles: the missing link for safe and efficient ultrasound triggered drug-delivery, J. Control. Release 152 (2011) 249–256.
[46] A. Bouakaz, A. Zeghimi, A.A. Doinikov, Sonoporation: concept and mechanisms, Advances in Experimental Medicine and Biology, 2016, pp. 175–189.
[47] C. Mannaris, L. Bau, M. Grundy, M. Gray, H. Lea-Banks, A. Seth, B. Teo, R. Carlisle, E. Stride, C.C. Coussios, Microbubbles, nanodroplets and gas-stabilizing solid particles for ultrasound-mediated extravasation of unencapsulated drugs: an exposure parameter optimization study, Ultrasound Med. Biol. 45 (2019) 954–967.
[48] Y. Hu, J.M.F. Wan, A.C.H. Yu, Membrane perforation and recovery dynamics in microbubble-mediated sonoporation, Ultrasound Med. Biol. 39 (2013) 2393–2405.
[49] I. Lentacker, S.C. De Smedt, J. Demeester, V. Van Marck, M. Bracke, N.N. Sanders, Lipoplex-loaded microbubbles for gene delivery: A trojan horse controlled by ultrasound, Adv. Funct. Mater. 17 (2007) 1910–1916.
[50] I. Lentacker, I. De Cock, R. Deckers, S.C. De Smedt, C.T.W. Moonen, Understanding ultrasound induced sonoporation: definitions and underlying mechanisms, Adv. Drug Deliv. Rev. 72 (2014) 49–64.
[51] E. Stride, C. Porter, A.G. Prieto, Q. Pankhurst, Enhancement of microbubble mediated gene delivery by simultaneous exposure to ultrasonic and magnetic fields, Ultrasound Med. Biol. 35 (2009) 861–868.
[52] R.M. Reilly, R. Kiarash, R.G. Cameron, N. Porlier, J. Sandhu, R.P. Hill, K. Vallis, A. Hendler, J. Gariépy, 111In-labeled EGF is selectively radiotoxic to human breast cancer cells overexpressing EGFR, J. Nucl. Med. 41 (2000) 429–438.
[53] A. Gabizon, H. Shmeeda, Y. Barenholz, Pharmacokinetics of pegylated liposomal

doxorubicin, Clin. Pharmacokinet. 42 (2003) 419–436.
[54] E. Thomas, J.U. Menon, J. Owen, I. Skaripa-Koukelli, S. Wallington, M. Gray, C. Mannaris, V. Kersemans, D. Allen, P. Kinchesh, S. Smart, R. Carlisle, K.A. Vallis, Ultrasound-mediated cavitation enhances the delivery of an EGFR-targeting liposomal formulation designed for chemo-radionuclide therapy, Theranostics 9 (2019) 5595–5609.
[55] C.D. Arvanitis, M. Bazan-Peregrino, B. Rifai, L.W. Seymour, C.C. Coussios, Cavitation-enhanced extravasation for drug delivery, Ultrasound Med. Biol. 37 (2011) 1838–1852.
[56] Y.-H. Chung, P.-H. Hsu, C.-W. Huang, W.-C. Hsieh, F.-T. Huang, W.-C. Chang, H. Chiu, S.-T. Hsu, T.-C. Yen, Evaluation of prognostic integrin α2β1 PET tracer and concurrent targeting delivery using focused ultrasound for brain glioma detection, Mol. Pharm. 11 (2014) 3904–3914.
[57] T.Y. Wang, J.W. Choe, K. Pu, R. Devulapally, S. Bachawal, S. Machtaler, S.M. Chowdhury, R. Luong, L. Tian, B. Khuri-Yakub, J. Rao, R. Paulmurugan, J.K. Willmann, Ultrasound-guided delivery of microRNA loaded nanoparticles into cancer, J. Control. Release 203 (2015) 99–108.
[58] J.J. Kwan, R. Myers, C.M. Coviello, S.M. Graham, A.R. Shah, E. Stride, R.C. Carlisle, C.C. Coussios, Ultrasound-propelled nanocups for drug delivery, Small (Weinheim an Der Bergstrasse, Germany) 11 (2015) 5305–5314.
[59] R. Myers, C. Coviello, P. Erbs, J. Foloppe, C. Rowe, J. Kwan, C. Crake, S. Finn, E. Jackson, J.-M. Balloul, C. Story, C. Coussios, R. Carlisle, Polymeric cups for cavitation-mediated delivery of oncolytic vaccinia virus, Mol. Ther. 24 (2016) 1627–1633.